Measurement 179 (2021) 109487

Contents lists available at ScienceDirect

Measurement

journal homepage: www.elsevier.com/locate/measurement

Defect-mediated sputtering process of boron nitride during high incident angle low-energy ion bombardment

Paweł Piotr Michałowski [a,*], Dawid Maciążek [b], Zbigniew Postawa [b], Piotr A. Caban [a], Sylwia Kozdra [a], Adrianna Wójcik [a,c], Jacek M. Baranowski [a]

[a] Łukasiewicz Research Network - Institute of Microelectronics and Photonics, Aleja Lotników 32/46, 02-668 Warsaw, Poland
[b] Smoluchowski Institute of Physics, Jagiellonian University, Łojasiewicza 11, 30-348 Kraków, Poland
[c] Faculty of Physics, Warsaw University, Pasteura 5, 02-093 Warsaw, Poland

ARTICLE INFO

Keywords:
Secondary ion mass spectrometry
Molecular dynamics
Sputtering
Boron nitride
2D materials

ABSTRACT

Further development of hexagonal boron nitride (hBN) towards electronic devices requires the application of precise analytical techniques. High incident angle (> 65°) secondary ion mass spectrometry has been recently developed, and allows to reach atomic depth. However, the procedure has been optimized experimentally, and thus computer simulations are needed to validate and comprehend the experiment. It is revealed that a sample without any defects cannot be sputtered in such conditions — all ions are reflected from the surface. Only defects, particularly vacancies, can act as erosion centers. After prolong bombardment (dose in the range of 10^{17} ions cm^{-2}), the number of defects and their sizes are sufficiently large that rapid removal of a top-most hBN layer can be observed. Computer simulations and additional experiments reveal that the sputtering process is defect-mediated and anisotropic — significantly more prominent along the incident direction.

1. Introduction

Two dimensional (2D) materials and their potential application into electronic devices are studied worldwide. One of the most promising representatives of this group is hexagonal boron nitride (hBN) with sp^2-hybridized atomic sheets of boron and nitrogen. Its structure is very similar to graphene, with a relatively low lattice mismatch (1.7% lattice mismatch), and high thermal conductivity. The major difference is a wide band gap of hBN, and thus, it can be potentially integrated with other 2D materials as a substrate and dielectric [1].

Before mass production and commercialization, the basic properties of 2D materials have to be examined. A variety of experimental methods are widely used to investigate the properties and quality of the hexagonal boron nitride samples: Raman spectroscopy is a useful tool for quick determination of the structural properties and quality of h-BN. The shift of the Raman peaks to higher and lower frequencies may give information about compressive and tensile stress, respectively [2]. Furthermore, Raman scattering can be used to determine the volume fraction of h-BN in the BN films [3]. Ultra-low Frequency Raman spectroscopy allows for the estimation of the number of layers in ultra-thin hBN [4,5]. Optical properties of the boron nitride have been studied experimentally, e.g., by means of Photoluminescence [6–8]. Useful information on an hBN structure such as distances between layers, average grain size, strain, crystal plane alignment can be delivered by X-ray diffraction investigations [9,10]. Additional support in structural characterization can be also obtained by scanning transmission electron microscopy images, which give a direct indication of the phase and quality of the structure [11,12]. Moreover, an inspection of the sample at the atomic scale can reveal the presence of structural defects [12,13]. Scanning electron microscopy and atomic force microscopy (AFM) are frequently used to investigate the morphology of the hBN samples [11,14]. Particularly, AFM has been widely employed to probe surface topography of hBN, e.g., to get quantitative information about the height of the characteristic wrinkles [15].

In our previous secondary ion mass spectrometry (SIMS) experiments on graphene [16–18], we have shown that measurements of 2D materials are non-trivial, and their presence can affect the ionization probability. We have also used SIMS to study the quality of hBN layers and the formation of carbon precipitation during the growth process of thin and smooth BN layers grown in a self-terminated growth mode [19–21]. We have described a measurement procedure that allowed us to reach atomic depth resolution [21]. First, the top layer is measured in a static SIMS regime. The total primary ion dose is sufficiently low, and less than 1% of the surface is damaged during the measurement. Then the sample is bombarded with a short pulse of primary ions at high incident angles. This ensures that weak van der Waals bonds are

* Corresponding author.
E-mail address: pawel.michalowski@imif.lukasiewicz.gov.pl (P.P. Michałowski).

https://doi.org/10.1016/j.measurement.2021.109487
Received 21 January 2021; Received in revised form 14 April 2021; Accepted 22 April 2021
Available online 26 April 2021

preferentially broken, and the top layer is sputtered, and the second layer is exposed for a static SIMS analysis. The repetition of these steps allows a precise characterization of each layer individually. This procedure, however, has been optimized experimentally, and a detailed description of the underlying physical processes responsible for such behavior during high incident angle ion bombardment are still unclear.

The impact of the incident angle was intensively studied in 70 s and 80 s by Wittmaack [22–26] and Magee [27–29]. The final conclusion was that incident angle in the range of 40° – 60° ensured high secondary ion yield and good depth resolution for most materials. Thus nowadays most instruments have fixed ion columns without a possibility to directly manipulate the incident angle and, as a consequence, its impact is seldom considered in recent studies. In most publications containing SIMS results the incident angle is not even reported. Recently Schiffmann [30] has presented a study for a broad range of incident angles (a sample can be tilted between 0° and 90° around the axis) and come to a conclusion that optimal value is 45° and 55° for carbon-based and nitride materials, respectively, which is in line with aforementioned studies by Wittmaack and Magee. However, the most prominent exceptions are proceedings of International Conferences on Secondary Ion Mass Spectrometry where authors regularly discuss this parameter [31–41]. Kataoka et al. [33] notice formation of ripples at the crater bottom during high incident angle bombardment. Merkulov et al. [41] discussed extra low impact energy SIMS procedures with varying incident angles, however, only the change of the impact energy is directly considered. Iida et al. [35] shows a particularly interesting study for C_{60}^+ primary beam. The conclusion is that the highest incident angle (76°) is the most suitable for molecular depth profiling because sputter induced damage of polymers is significantly reduced.

Computer simulation are not limited by instruments' design and thus the influence of the incident angle is often considered [42–46]. Thus in this work molecular dynamics computer simulations combined with experimental measurements are used to study in detail the sputtering process of boron nitride during high incident angle low-energy ion bombardment. In this way, it is possible to obtain valuable knowledge about the interaction of primary ions with hBN layers but also indirectly about properties of the hexagonal boron nitride itself.

2. Experimental setup

2.1. Sample preparation

Boron nitride films were grown in the self-terminated growth mode investigated by Paduano et al. [47,48] and exact growth parameters are presented in our previous studies [19,21]. Argon was used as a carrier gas and thickness of BN sample was about 1.8 nm which corresponds to 6 layers.

2.2. Secondary ion mass spectrometry

SIMS measurements were performed employing the CAMECA SC Ultra instrument and the details about measurement procedure are presented in our previous study [21]. The most important changes, when compared to standard SIMS experiments, were the ultra low impact energy of 100 eV and a high incident angle (65 – 77°) for a Cs^+ primary beam and negative secondary ion polarity. No significant differences has been observed for various angles and thus the same value as in our previous study has been chosen (69°) for the following experiments.

2.3. Computer simulations

A detailed description of the molecular dynamics computer simulations used to model cluster bombardment can be found elsewhere [49].

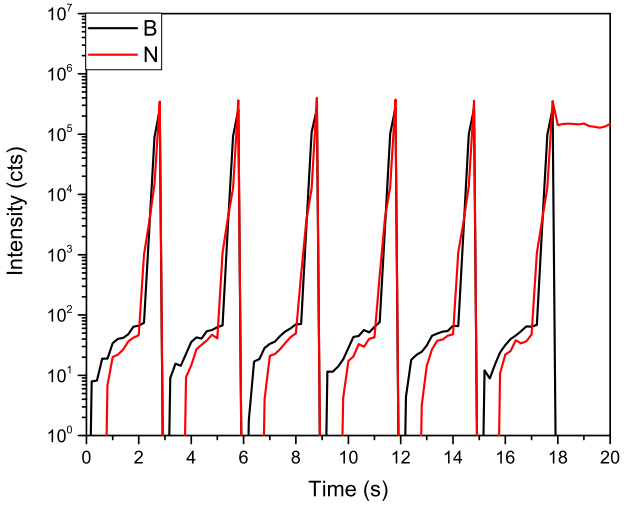

Fig. 1. A depth profile showing B and N signal for ultra low impact energy and high incident angle cesium bombardment. In the beginning, the intensity of both signals is very low. At one point, they rapidly increase and shortly thereafter vanish. The number of such cycles corresponds to the number of hBN layers, which indicates that each hBN layer is sputtered independently. The figure is available in csv format in Supplementary Materials.

Briefly, the motion of particles is determined by integrating the Hamilton equations of motion. The forces between boron and nitrogen atoms in the hexagonal Boron Nitride (h-BN) layer are described by BN-ExTeP potential [50]. The Lennard-Jones potential describes the interlayer interactions. These potential parameters are fitted, so the relaxed sample has 3.33 Å interlayer distance, and interlayer binding energy per atom is equal to 85.9 meV [51]. Interactions involving cesium projectile (Cs-Cs, Cs-B, Cs-N) are described by the ZBL potential [52]. All simulations are performed with the large-scale atomic/molecular massively parallel simulator code (LAMMPS) [53].

The simulated sample consisted of 5 layers of h-BN in the AA′ stacking mode [51] with a size 135 Å × 104 Å × 17 Å. Periodic boundary conditions are used in the lateral directions, with the bottom-most layer fixed in place. A thermal bath is applied to the second and third layers from the bottom to keep the system at$T = 300$ K. The sputtering process is modeled as a series of sequential impacts, where each impact consisted of 3 steps. In step one, the Cs atom is created above the sample surface at a randomly selected position with a velocity vector corresponding to the beam parameters used in the experiment (kinetic energy 100 eV, impact angle 69°). In the next step, the evolution of the system is simulated for 10 ps. During this phase, sputtering, atom redistribution, and the chemical effects are taking place. In the final step, the additional thermal bath is applied to all layers to remove residual stress before the next impact.

3. Results and discussion

In our previous work [21], high incident angle bombardment was used only for removal of subsequent hBN layers, and the detector was switched off because it was difficult to optimize the extraction of secondary ions in such non-trivial conditions. Since then, we have, however, overcome this problem (by finely tuning the extraction parameters) and thus we have been able to create full depth profiles during the high incident angle bombardment — see Fig. 1. As it can be immediately seen, the result is periodic and consists of six almost identical parts corresponding to six layers of hBN. For samples with a bigger number of layers the result is analogous. At the end of a profile, the B signal vanishes, whereas the N signal reaches a constant value (the substrate was nitridated before the growth process). However, contrary to a typical SIMS result, both signals change a lot during the sputtering process of hBN layers:

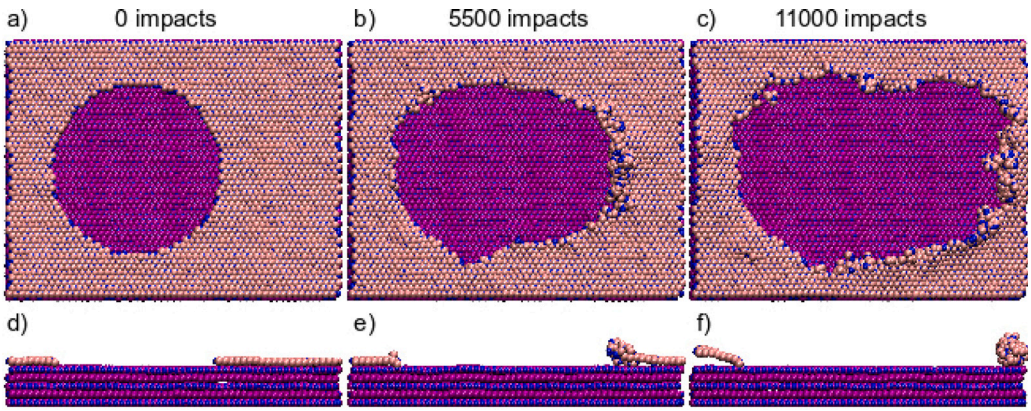

Fig. 2. Visualization of the evolution of the h-BN sample with initial circular defect undergoing continuous bombardment with different doses: (a,d) 0 ions cm^{-2}, (b, (e) 3.9×10^{15} ions cm^{-2}, (c, (f) 7.8×10^{15} ions cm^{-2}. The system top view is shown in panels (a–c), while panels (d–f) present the cross-sectional view. Nitrogen atoms are represented as blue spheres, and boron atoms are represented as pink (topmost layer) and violet (2th–5th layer) spheres. A movie showing evolution of this system can be found in Supplementary Materials. (For interpretation of the references to color in this figure legend, the reader is referred to the web version of this article.)

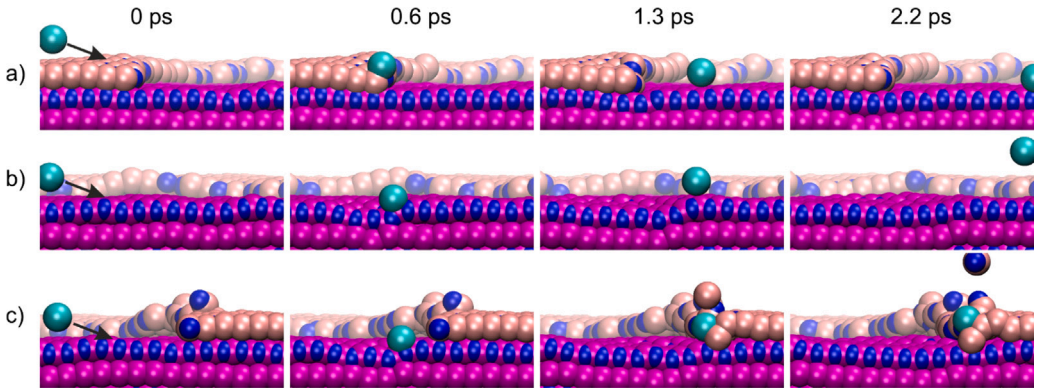

Fig. 3. Temporal evolution of the BN surface bombarded by 100 eV Cs projectile at 69° angle of incidence for impacts occurring on (a) the topmost layer near the defect edge, b the locally undamaged part of the exposed portion of the second layer far from the defect edge, and (c) the exposed second layer near the defect edge. The atom coloring scheme is the same as in Fig. 2. Movies showing these impacts can be found in Supplementary Materials.

- at the beginning, only a minimal number of boron counts can be registered;
- after some time, nitrogen counts can also be registered;
- both signals steadily increase over about two seconds, but their intensities remain very low (less than one hundred counts);
- at one point, both signals start to increase rapidly, reaching more than three orders of magnitude higher values within less than half a second (it may seem that the nitrogen signal increases faster but there is only a single data point difference which originates from the fact that secondary ions are measured sequentially);
- both signals drop to zero even more rapidly.

The fact that the boron signal is the first to be registered is easy to explain. Cesium is used as primary ions. The electronegativity difference between cesium and nitrogen is 2.25, whereas 1.25 between cesium and boron. Electronegativity is a concept that describes the tendency of an atom to attract a shared pair of electrons towards itself. The more significant is the electronegativity difference, the greater is the tendency to attract electrons by an atom of a given element, even at the expense of another. Furthermore, the atomic radius of boron (87 pm) is bigger than of nitrogen (56 pm), and, thus, much larger cesium (298 pm) may preferentially sputter a boron atom and take its place in the hBN lattice. However, such simple consideration cannot explain why at some point both, signals increase rapidly and vanish entirely in a split second.

It is also important to emphasize that the quality of the profile presented on Fig. 1 does not deteriorate even for much thicker samples (more than 60 layers of hBN) — each and every periodic feature is of the same quality. It suggests that each layer is sputtered individually and there is no atomic redistribution between neighboring layers.

To gain better insight, we have performed computer simulations for two systems of multi-layer hBN. The first system is a pristine sample without any defects. After 7000 impacts (dose 5×10^{15} ions cm^{-2}), not a single defect is created in the sample. All impacting projectiles are reflected from the surface without introducing any permanent surface modification. This is in line with work of Iida et al. [35] where it has been presented that for high incident angle bombardment the sputter induced damage is significantly reduced.

For the second system, we have introduced a circular defect with a radius of 50 Å to the topmost layer (see Fig. 2a). The evolution of the system undergoing 11 000 impacts (dose equal to 7.8×10^{15} ions cm^{-2}) is shown in Fig. 2 and corresponding Animation. In this case, projectiles are bombarding the surface from left to right. It is evident that this time, the geometry of the topmost layer is modified by projectile impacts. The defect evolution of this layer displays a strong anisotropy of erosion on the defect right-hand side. Additionally, continuous bombardment does not alter the geometry of the second layer. This result corresponds very well to study of Kataoka et al. [33] where formation of ripples during high incident angle bombardment has been reported.

Before exploring the kinematics of individual cases of a projectile impact, we should mention the factors that will limit the effectiveness of energy transfer between the projectile and individual surface atoms. The first factor is the large mass difference between the projectile atom and the substrate atoms. Even in the most favorable case of a central

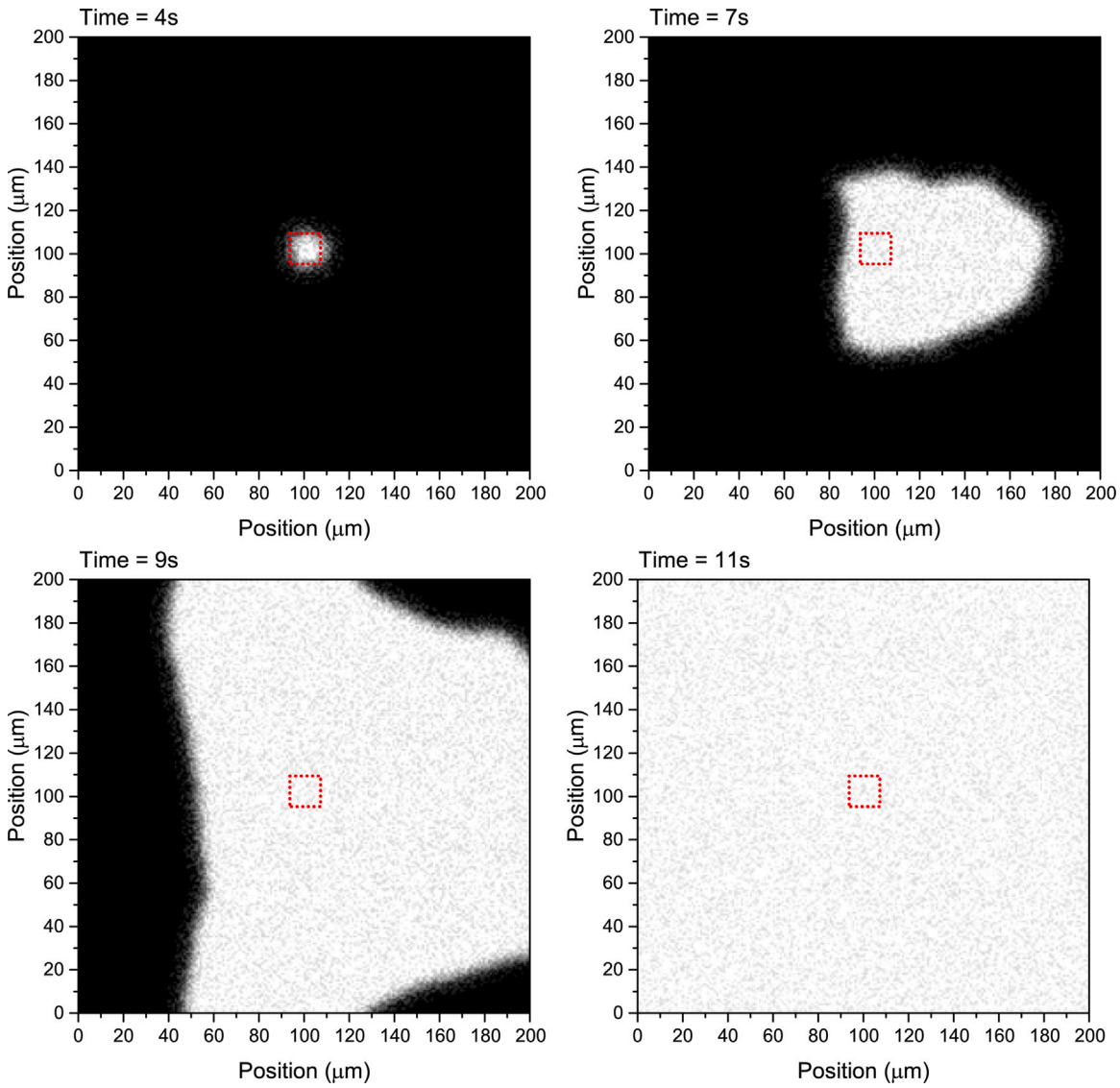

Fig. 4. Aluminum secondary ions distribution maps show at what time all hBN layers are sputtered, and the substrate is fully exposed. The red dotted square shows the location of the pre-bombardment area. For this region, the substrate is exposed after four seconds. The rest of the sputtering process is asymmetrical: layers at the right side are sputtered faster, which corresponds to the direction of primary ions incidence: from left to right. Four selected frames are presented. Full animation of these data (one frame per second) can be found in Supplementary Materials.

two-body collision, only around 26 eV and 34 eV of kinetic energy would be transferred to the boron or nitrogen atoms, respectively. The second factor is related to the many-body nature of interactions. The projectile impacts at the surface at a high angle of incidence. As a result, it will never transfer its energy to one atom but share it among several atoms. To explain erosion anisotropy, we consider three different cases of the impact location. In the first case, impact occurs on the topmost layer near the defect edge, as shown in Fig. 3a and corresponding Animation. The projectile arrives at a high incidence angle. It agitates several atoms losing its kinetic energy before hitting the atom located at the edge. The atoms on the left also shield this atom, so the collision usually occurs with a large impact parameter, limiting the efficiency of energy transfer. Furthermore, a part of the velocity gained by this atom is directed towards the second layer and shared with atoms located in deeper layers. As a result, the energy of the impacted atoms is not sufficient to let this atom to eject, and such an impact results in a minimal chance of sputtering. In the second case, the impact occurs on the undamaged part of the topmost layer or the exposed portion of the second layer far from the defect edge. The latter case is visualized in Fig. 3b and corresponding Animation. Due to a high angle of incidence, normal component of projectile velocity is low, and the projectile slides over the perfect surface distorting its geometrical structure only temporarily. No sputtering or defect formation occurs in both these situations, as observed in simulations performed on the pristine sample. In the third case, illustrated in Fig. 3c and corresponding Animation, the impact occurs on the exposed second layer near the defect edge. The initial behavior of the projectile is the same as the impact on the perfect flat surface. The projectile only temporarily distorts the surface, sliding over it. However, in this case, it collides with the first layer atom located at the edge of a defect on its way out. The transmitted momentum is directed upwards. The collision can be central, and the energy transfer is efficient. The atom is forced to eject. This scenario can only occur for projectiles impacting the surface within a specific distance of approximately 6 Å between the projectile impact point and the ejected atom initial location. If the distance is larger than this specific distance, the scenario is described in Fig. 3b. Finally, it should be noted that our simulations do not show how the initial defects are created. We believe that this could be linked to possible beam imperfections (particularly presence of ions with lower incident angles) or thermodynamical processes of statistical nature, which occur at the time scale we cannot model.

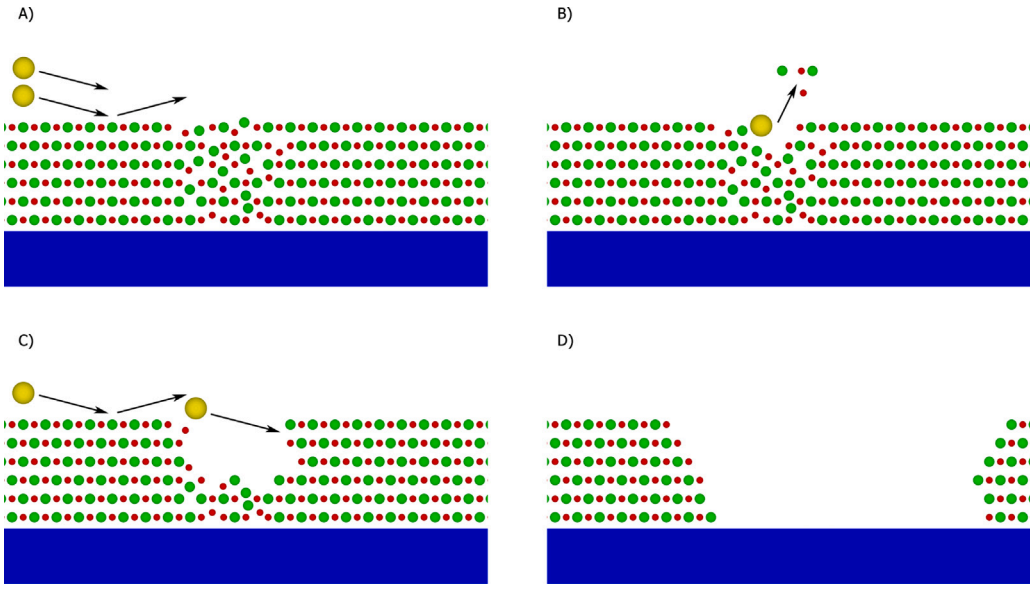

Fig. 5. Schematic visualization of a high incident angle cesium ions bombardment of a pre-defected sample. For such conditions, most primary ions bounce off the surface (part A). Those projectiles which hit a pre-bombarded defected area, cause the sputtering of hBN layers (part B). The further sputtering process is asymmetrical. Ions still bounce off the surface at one side, whereas collision at effectively lower incident angle at the other side (part C) causes that this side is sputtered much faster (part D). For a pre-defected sample, the layer-by-layer nature of the sputtering process is no longer preserved.

To verify these conclusions, we have devised an additional experiment: a high energy beam (13 keV) with a standard incident angle (40°) and a very low density (the total dose below 10^{12} atoms cm^{-2}) has been used to pre-bombard a very small area (15 × 15 microns). For such a low dose, it is not possible to sputter many atoms, but such a high impact energy ensures that a lot of defects have been created in this area. Then high incident angle beam has been used, but instead of boron or nitrogen, we have decided to measure ion images of aluminum signal (lateral distribution). This element is not present in hBN layers, and thus no signal is expected at the beginning of the experiment. However, after the removal of all hBN layers, the sapphire is exposed, and the Al signal can be registered.

The result presented in Fig. 4 is indeed very interesting. As expected, no Al signal is observed at the beginning of the experiment. But just after four seconds, the substrate in the region pre-bombarded by a high energy beam is fully exposed (without pre-bombardment, it takes eighteen seconds to fully remove six hBN layers). Other regions are exposed with time but, similarly to computer simulations, in a very asymmetrical manner: material located to the right of the pre-bombarded area is sputtered much faster than to the left. This is not surprising as this corresponds to the direction of primary ions incidence: from left to right. Therefore primary ions can sputter this part of a sample much easier because the effective collision angle is much lower. This is schematically shown in Fig. 5. It should be also emphasized that the substrate is fully exposed everywhere just after eleven seconds — seven seconds faster than for a case without pre-bombardment. This is not surprising as the introduction of defects to all six layers causes the layer-by-layer nature of the sputtering process to be no longer preserved. A simultaneous sputtering of several hBN layers is naturally a faster process.

4. Conclusions

The Molecular dynamics computer simulations are combined with the experimental measurements to delineate the processes leading to layer-by-layer sputtering of hexagonal boron nitride with low-energy high incidence angle bombardment with cesium projectiles. It has been found that for such non-trivial bombardment conditions the evolution of the sputtering process is strongly affected by the presence of defects, particularly vacancies. It should be emphasized that computer simulations are in excellent agreement with experiments, and they both reveal anisotropic nature of the sputtering process — it is significantly more prominent along the incident direction. Such an effect has not been observed for standard SIMS experiments with moderate/low incident angles.

These results finally allow to explain the shape of the depth profile presented in Fig. 1. Every realistic sample contains some vacancies and other defects, and while they may not be as big as it has been assumed in computer simulations, these defects act as erosion centers — in the initial state of the ion bombardment, these defects become bigger, and thus more and more atoms are sputtered (a steady increase of boron and nitrogen signals). After some time, the number and the size of these defects are large enough that the whole layer can be sputtered very quickly (a very rapid increase of both signals). Then a fresh layer is exposed, and thus the entire process starts again (signals drop to zero).

CRediT authorship contribution statement

Paweł Piotr Michałowski: Conceptualization, Methodology, Validation, Formal analysis, Investigation, Writing - original draft, Writing - review & editing, Visualization, Funding acquisition. **Dawid Maciążek:** Software, Validation, Formal analysis, Data curation. **Zbigniew Postawa:** Software, Validation, Formal analysis, Data curation, Writing - review & editing, Funding acquisition. **Piotr A. Caban:** Formal analysis, Resources, Investigation. **Sylwia Kozdra:** Formal analysis, Visualization. **Adrianna Wójcik:** Formal analysis, Visualization. **Jacek M. Baranowski:** Formal analysis, Writing - review & editing.

Declaration of competing interest

The authors declare that they have no known competing financial interests or personal relationships that could have appeared to influence the work reported in this paper.

Acknowledgments

This work was supported by the Polish National Science Centre within SONATA 14 2018/31/D/ST5/00399 and OPUS 17 2019/33/B/ST4/01778 projects. MD simulations were performed at the PLGrid Infrastructure.

Appendix A. Supplementary data

Supplementary material related to this article can be found online at https://doi.org/10.1016/j.measurement.2021.109487.

References

[1] C. Dean, A. Young, I. Meric, L. Wang, S. Sorgenfrei, K. Watanabe, T. Taniguchi, P. Kim, K. Shepard, J. Hone, Boron nitride substrates for high-quality graphene electronics, Nature Nanotechnol. 5 (2010) 3209.

[2] Y. Kobayashi, T. Akasaka, Hexagonal BN epitaxial growth on (0001) sapphire substrate by MOVPE, J. Cryst. Growth 310 (23) (2008) 5044–5047.

[3] S. Reich, A.C. Ferrari, R. Arenal, A. Loiseau, I. Bello, J. Robertson, Resonant Raman scattering in cubic and hexagonal boron nitride, Phys. Rev. B 71 (2005) 205201.

[4] I. Stenger, L. Schué, M. Boukhicha, B. Berini, B. Plaçais, A. Loiseau, J. Barjon, Low frequency Raman spectroscopy of few-atomic-layer thick hBN crystals, 2d Mater. 4 (3) (2017) 031003.

[5] L. Schué, I. Stenger, F. Fossard, A. Loiseau, J. Barjon, Characterization methods dedicated to nanometer-thick hBN layers, 2d Mater. 4 (1) (2016) 015028.

[6] M.G. Silly, P. Jaffrennou, J. Barjon, J.-S. Lauret, F. Ducastelle, A. Loiseau, E. Obraztsova, B. Attal-Tretout, E. Rosencher, Luminescence properties of hexagonal boron nitride: Cathodoluminescence and photoluminescence spectroscopy measurements, Phys. Rev. B 75 (2007) 085205.

[7] J. Wu, W.-Q. Han, W. Walukiewicz, J.W. Ager, W. Shan, E.E. Haller, A. Zettl, Raman Spectroscopy and time-resolved photoluminescence of BN and bxcynz nanotubes, Nano Lett. 4 (4) (2004) 647–650.

[8] K. Watanabe, T. Taniguchi, H. Kanda, Direct-bandgap properties and evidence for ultraviolet lasing of hexagonal boron nitride single crystal, Nature Mater. 3 (6) (2004) 404–409.

[9] B. Matović, J. Luković, M. Nikolić, B. Babić, N. Stanković, B. Jokić, B. Jelenković, Synthesis and characterization of nanocrystaline hexagonal boron nitride powders: XRD and luminescence properties, Ceram. Int. 42 (15) (2016) 16655–16658.

[10] M. Öz, N.K. Saritekın, Ç. Bozkurt, G. Yildirim, Synthesis of highly ordered hBN in presence of group i/IIA carbonates by solid state reaction, Cryst. Res. Tech. 51 (6) (2016) 380–392.

[11] X. Li, S. Sundaram, Y. El Gmili, T. Ayari, R. Puybaret, G. Patriarche, P.L. Voss, J.P. Salvestrini, A. Ougazzaden, Large-area two-dimensional layered hexagonal boron nitride grown on sapphire by metalorganic vapor phase epitaxy, Cryst. Growth Des. 16 (6) (2016) 3409–3415.

[12] M.L. Odlyzko, K.A. Mkhoyan, Identifying hexagonal boron nitride monolayers by transmission electron microscopy, Microsc. Microanal. 18 (3) (2012) 558–567.

[13] N.L. McDougall, J.G. Partridge, R.J. Nicholls, S.P. Russo, D.G. McCulloch, Influence of point defects on the near edge structure of hexagonal boron nitride, Phys. Rev. B 96 (2017) 144106.

[14] K.P. Sharma, S. Sharma, A. Khaniya Sharma, B. Paudel Jaisi, G. Kalita, M. Tanemura, Edge controlled growth of hexagonal boron nitride crystals on copper foil by atmospheric pressure chemical vapor deposition, CrystEngComm 20 (2018) 550–555.

[15] D. Chugh, J. Wong-Leung, L. Li, M. Lysevych, H.H. Tan, C. Jagadish, Flow modulation epitaxy of hexagonal boron nitride, 2d Mater. 5 (4) (2018) 045018.

[16] P.P. Michałowski, W. Kaszub, I. Pasternak, W. Strupinski, Graphene enhanced secondary ion mass spectrometry (GESIMS), Sci. Rep. 7 (2017) 7479.

[17] P.P. Michałowski, I. Pasternak, W. Strupinski, Contamination-free ge-based graphene as revealed by graphene enhanced secondary ion mass spectrometry (GESIMS), Nanotechnology 29 (2018) 015702.

[18] P.P. Michałowski, I. Pasternak, P. Ciepielewski, F. Guinea, W. Strupinski, Formation of a highly doped ultra-thin amorphous carbon layer by ion bombardment of graphene, Nanotechnology 29 (2018) 305302.

[19] P. Caban, D. Teklińska, P. Michałowski, J. Gaca, M. Wójcik, J. Grzonka, P. Ciepielewski, M. Możdżonek, J. Baranowski, The role of hydrogen in carbon incorporation and surface roughness of MOCVD-grown thin boron nitride, J. Cryst. Growth 498 (2018) 71–76.

[20] P. Caban, P. Michalowski, I. Wlasny, J. Gaca, M. Wojcik, P. Ciepielewski, D. Teklinska, J. Baranowski, Carbon incorporation in boron nitride grown by MOCVD under N2 flow, J. Alloys Compd. 815 (2020) 152364.

[21] P.P. Michałowski, P. Caban, J. Baranowski, Secondary ion mass spectrometry investigation of carbon grain formation in boron nitride epitaxial layers with atomic depth resolution, J. Anal. Atom. Spectrom. 34 (2019) 848–853.

[22] K. Wittmaack, Secondary ion yield variations due to cesium implantation in silicon, Surf. Sci. 126 (1) (1983) 573–580.

[23] K. Wittmaack, Impact-energy dependence of atomic mixing and selective sputtering of light impurities in cesium-bombarded silicon, Nucl. Instrum. Methods Phys. Res. B 209–210 (1983) 191–195.

[24] K. Wittmaack, The effect of the angle of incidence on secondary ion yields of oxygen-bombarded solids, Nucl. Instrum. Methods Phys. Res. B 218 (1) (1983) 307–311.

[25] K. Wittmaack, Beam-induced broadening effects in sputter depth profiling, Vacuum 34 (1) (1984) 119–137.

[26] K. Wittmaack, Influence of the impact angle on the depth resolution and the sensitivity in SIMS depth profiling using a cesium ion beam, J. Vac. Sci. Technol. A 3 (3) (1985) 1350–1354.

[27] C.W. Magee, W.L. Harrington, R.E. Honig, Secondary ion quadrupole mass spectrometer for depth profiling—design and performance evaluation, Rev. Sci. Instrum. 49 (4) (1978) 477–485.

[28] C.W. Magee, S.A. Cohen, D.E. Voss, D.K. Brice, Depth distributions of low energy deuterium implanted into silicon as determined by sims, Nucl. Instrum. Methods 168 (1) (1980) 383–387.

[29] C.W. Magee, R.E. Honig, Depth profiling by SIMS—depth resolution, dynamic range and sensitivity, Surf. Interface Anal. 4 (2) (1982) 35–41.

[30] K.I. Schiffmann, SIMS Depth profile analysis of tribological coatings on curved surfaces: Influence of ion impact angle and take-off angle on ion yield and on the quantitative analysis of chemical composition, Surf. Interface Anal. 51 (7) (2019) 703–711.

[31] M. Bersani, D. Giubertoni, M. Barozzi, E. EIacob, L. Vanzetti, M. Anderle, P. Lazzeri, B. Crivelli, F. Zanderigo, D-SIMS and tof-SIMS quantitative depth profiles comparison on ultra thin oxynitrides, Appl. Surf. Sci. 203–204 (2003) 281–284.

[32] Y. Homma, A. Takano, Y. Higashi, Oxygen-ion-induced ripple formation on silicon: evidence for phase separation and tentative model, Appl. Surf. Sci. 203–204 (2003) 35–38.

[33] Y. Kataoka, K. Yamazaki, M. Shigeno, Y. Tada, K. Wittmaack, Surface roughening of silicon under ultra-low-energy cesium bombardment, Appl. Surf. Sci. 203–204 (2003) 43–47.

[34] A. Villegas, Y. Kudriavtsev, A. Godines, R. Asomoza, Work function change caused by alkali ion sputtering, Appl. Surf. Sci. 203–204 (2003) 94–97.

[35] S.-i. Iida, T. Miyayama, N. Sanada, M. Suzuki, G.L. Fisher, S.R. Bryan, Optimizing C60 incidence angle for polymer depth profiling by tof-SIMS, Surf. Interface Anal. 43 (1–2) (2011) 214–216.

[36] A. Merkulov, P. Peres, D.J. Larson, M. Schuhmacher, Quantitative low energy depth profiling of sige laterally nonuniform structures, J. Vac. Sci. Technol. B 36 (3) (2018) 03F121.

[37] Y. Mazel, E. Nolot, J.-P. Barnes, M. Charles, R. Bouveyron, M. Mrad, A. Tempez, S. Legendre, Multitechnique elemental depth profiling of inalgan and inaln films, J. Vac. Sci. Technol. B 36 (3) (2018) 03F119.

[38] M.K.I. Senevirathna, M. Vernon, G.A. Cooke, G.B. Cross, A. Kozhanov, M.D. Williams, Analysis of useful ion yield for si in gan by secondary ion mass spectrometry, J. Vac. Sci. Technol. B 38 (4) (2020) 044002.

[39] M.K.I. Senevirathna, M.D. Williams, G.A. Cooke, A. Kozhanov, M. Vernon, G.B. Cross, Analysis of useful ion yield for the Mg dopant in gan by quadrupole—SIMS, J. Vac. Sci. Technol. B 38 (3) (2020) 034015.

[40] N. Nishida, M. Sakurai, D. Kato, H.A. Sakaue, Observation of light and secondary ion emissions from surfaces irradiated with highly charged ions, J. Vac. Sci. Technol. B 38 (4) (2020) 044006.

[41] A. Merkulov, P. Peres, K. Soulard, D.J. Larson, K. Sivaramakrishnan, Improvement of extra low impact energy SIMS data reduction algorithm for process control, J. Vac. Sci. Technol. B 38 (5) (2020) 053201.

[42] B. Weidtmann, S. Hanke, A. Duvenbeck, A. Wucher, Influence of the polar angle of incidence on secondary ion formation in self-sputtering of silver, Surf. Interface Anal. 43 (1–2) (2011) 24–27.

[43] L. Rzeznik, R. Paruch, B.J. Garrison, Z. Postawa, Sputtering of a coarse-grained benzene and ag(111) crystals by large ar clusters – effect of impact angle and cohesive energy, Surf. Interface Anal. 45 (1) (2013) 27–30.

[44] M. Golunski, Z. Postawa, Effect of kinetic energy and impact angle on carbon ejection from a free-standing graphene bombarded by kilo-electron-volt C60, J. Vac. Sci. Technol. B 36 (3) (2018) 03F112.

[45] M. Kański, Z. Postawa, Effect of the impact angle on the kinetic energy and angular distributions of β-carotene sputtered by 15 kev ar2000 projectiles, Anal. Chem. 91 (14) (2019) 9161–9167.

[46] M. Gołuński, S. Hrabar, Z. Postawa, Mechanisms of molecular emission from phenylalanine monolayer deposited on free-standing graphene bombarded by C60 projectiles, Appl. Surf. Sci. 539 (2021) 148259.

[47] Q.S. Paduano, M. Snure, J. Bondy, T.W.C. Zens, Self-terminating growth in hexagonal boron nitride by metal organic chemical vapor deposition, Appl. Phys. Express 7 (7) (2014) 071004.

[48] Q. Paduano, M. Snure, D. Weyburne, A. Kiefer, G. Siegel, J. Hu, Metalorganic chemical vapor deposition of few-layer sp2 bonded boron nitride films, J. Cryst. Growth 449 (2016) 148–155.

[49] B.J. Garrison, Z. Postawa, Computational view of surface based organic mass spectrometry, Mass Spectrom. Rev. 27 (4) (2008) 289–315.

[50] J.H. Los, J.M.H. Kroes, K. Albe, R.M. Gordillo, M.I. Katsnelson, A. Fasolino, Extended tersoff potential for boron nitride: Energetics and elastic properties of pristine and defective h-BN, Phys. Rev. B 96 (2017) 184108.

[51] O. Hod, Graphite and hexagonal boron-nitride have the same interlayer distance. Why?, J. Chem. Theory Comput. 8 (4) (2012) 1360–1369.

[52] J.F. Ziegler, J.P. Biersack, The stopping and range of ions in matter, in: D.A. Bromley (Ed.), Treatise on Heavy-Ion Science: Volume 6: Astrophysics, Chemistry, and Condensed Matter, Springer US, Boston, MA, 1985, pp. 93–129.

[53] S. Plimpton, Fast parallel algorithms for short-range molecular dynamics, J. Comput. Phys. 117 (1) (1995) 1–19.